ChemistrySelect

Research Article
doi.org/10.1002/slct.202304078

Chemistry Europe
European Chemical Societies Publishing

www.chemistryselect.org

Assessment of Electromagnetic Shielding Efficacy of Magnetic Metal Oxide Nanoparticles and their Application in Electromagnetic Shielding Paints

Gülay Demirci,[a] Serdar Okuyucu,[b] Numan Hoda,[c] and Önder Topel*[a]

People are continuously exposed to electromagnetic waves emitted by mobile phones, base stations, computers, household electrical appliances, and nearby devices. Shielding against electromagnetic radiation is of great importance to avoid potential adverse effects on human health. This study addresses the development of electromagnetic shielding paints containing magnetic metal oxide nanoparticles. Magnetic metal oxide nanoparticles with a spinel ferrite structure, namely Fe_3O_4, $CoFe_2O_4$, and $SnFe_2O_4$, were synthesized using the co-precipitation method. Their structural, morphological, and magnetic properties were characterized through FTIR, XRD, TEM, and VSM measurements. Electromagnetic shielding efficacy was assessed within the 3.5–12.5 GHz frequency range using waveguide measurements. Notably, pure magnetic metal oxide nanoparticles exhibited limited shielding efficiency, but incorporating conductive materials like multi-walled carbon nanotubes improved the efficacy. Optimization studies, involved adjusting the nanoparticle-to-carbon nanotube ratios and coating thickness, demonstrated the best shielding to be with 50:10 [MFe_2O_4:PEG]:mwcnt ratio (M:Fe, Co, Sn) and 0.720 mm thickness, achieving up to 99% of radiation shielding. The subsequent incorporation of the optimized magnetic composites into a water-based wall paint at a 1:2 weight ratio demonstrated their effectiveness in shielding, successfully blocking 84% of incoming radiation.

Introduction

In the last 50 years, electronic devices have become an integral part of our daily lives due to remarkable advancements in science and technology. These devices emit electromagnetic waves into the environment constantly. We are continuously exposed to electromagnetic radiation not only from the electronic devices in our immediate surroundings, such as microwave ovens, vacuum cleaners, laptops, and mobile phones, but also from high-voltage lines, base stations, high-tech diagnostic, and treatment devices, and so on. The resultant pollution of electromagnetic radiation has now reached such limits that it has the potential to negatively impact human life. The World Health Organization (WHO) has declared that electromagnetic radiation become the root cause of many health issues, both proven and unproven.[1] Studies have shown that prolonged exposure to electromagnetic waves can result in severe health problems, such as weakness, high blood pressure, headaches, weakened immune systems, and even cancer.[2] In 2001, the International Agency for Research on Cancer (IARC) classified electromagnetic fields as possible class 2B carcinogens,[3] and a meeting on the "Sensitivity of Children to Electromagnetic Fields," organized by WHO and Gazi University, Ankara-Turkey in 2004, reported that electromagnetic radiation doubles the risk of leukemia in children.[4] These findings highlight the significance of the potential impact of electromagnetic radiation on human health, underlining the need to of being shielded from the radiation from electronic device. Furthermore, in addition to health concerns, shielding electromagnetic radiation is also vital for military and defense applications. With the advent of technology that allows the transformation of electromagnetic waves emitted by computers into usable data without the need for cables or networks, shielding electromagnetic waves has become a critical need for the security of confidential government information and documents.

Electromagnetic shielding refers to the process of partially or completely blocking the propagation of electromagnetic radiation using a shielding material.[5] The effectiveness of electromagnetic shielding is determined by a parameter called the shielding efficiency (SE), also referred to as the "shielding effectiveness" (SE), expressed in decibels (dB). Shielding efficiency (SE) can be defined as a parameter that quantifies a material's ability to obstruct electromagnetic (EM) energy of a specific frequency as it passes through and calculated using Equation 1.

[a] G. Demirci, Assoc. Prof. Dr. Ö. Topel
Department of Chemistry
Akdeniz University
07058 Antalya, Turkey
E-mail: ondertopel@akdeniz.edu.tr

[b] S. Okuyucu
Department of Electrical and Electronical Engineering
Antalya Bilim University
07190, Antalya, Turkey

[c] Prof. Dr. N. Hoda
Department of Material Sciences and Engineering
Akdeniz University
07058, Antalya, Turkey

Supporting information for this article is available on the WWW under https://doi.org/10.1002/slct.202304078

$$SE = 10x\log\left(\frac{P_i}{P_t}\right) = 20x\log\left(\frac{E_i}{E_t}\right) = 20x\log\left(\frac{H_i}{H_t}\right) \quad (1)$$

Here P, E and H refer to power, electric and magnetic field intensities while i and t represent the incident and transmitted components, respectively.[5] In order for shielding to be effective, the material should ideally reduce and/or absorb the energy of the electromagnetic wave. When electromagnetic radiation passes through a material of thickness t, three distinct mechanisms occur; (*i*) reflection, which arises from the interaction between the incoming EM wave and charge carriers (electrons or holes) in the material, (*ii*) absorption, which depends on the thickness of the material, and multiple reflections, which occur due to secondary reflections within the material.[5,6] Therefore, the overall shielding efficiency (SE) of a material is the sum of the contributions from all three mechanisms, as follows:

$$SE = SE_{absorption} + SE_{reflection} + SE_{multiple\ internal\ reflections} \quad (2)$$

The level of attenuation of electromagnetic radiation is typically expressed as the shielding percentage (% shielding or S_p), which is based on the shielding efficiency (SE) calculated by Eq. 2:

$$S_p\ (\%\ \text{shielding}) = (1 - 10^{-SE/20}) \times 100 \quad (3)$$

The effectiveness of electromagnetic shielding is then quantified based on the value of S_p as calculated from Eq. 3. Two key properties that affect the EM shielding performance of materials are magnetism and conductivity, and they are closely related to the frequency of the radiation.[7] At low frequencies, the shielding capability of the material increases with its magnetic properties. The magnetic property of a material enhances the absorption of EM radiation while reducing reflections. Conversely, the conductivity of a material enhances the shielding performance by affecting the electrical field component of EM radiation through reflection. This phenomenon is particularly practical at high frequencies. Additionally, the thickness of a material affects the shielding performance; thicker materials are required to shield the magnetic field component of EM radiation, while thinner materials are sufficient for the electrical field component of the radiation.[7]

Shielding electromagnetic waves is of great importance, and consequently, many studies have been conducted in this field. The most desirable features in such studies are low density and cost. Conductive materials have been found to be particularly effective in shielding electromagnetic waves. Most of the studies have employed either metals or composites for this purpose. While this approach has been effective in shielding, it has resulted in increased costs, high specific gravity, and susceptibility to corrosion. Furthermore, the use of such materials has been limited due to difficulties associated with electricity grounding.[8] Moreover, it is considered a disadvantage that metal-based conductive materials reflect rather than absorb electromagnetic waves, resulting in electromagnetic wave pollution. Despite this issue, their widespread use persists due to their exceptional conductivity.[9] Alternatively, some composite materials through the incorporation of graphite and boron into a conductive polymer were prepared and investigated their effectiveness in shielding electromagnetic waves. Despite the advantages offered by these materials such as their lightweight and flexible nature, their inferior shielding properties compared to metals have restricted their application in certain areas, as noted by previous research.[10] Magnetite and metal oxide-magnetite blends have been employed in several investigations.[11] The feasibility of using composite materials comprising graphene oxide, magnetite and conductive polymers has also been explored. In the studies, conductive polymer materials have typically yielded superior results in terms of high reflectivity and absorption of electromagnetic radiation.[12]

The shielding of high-frequency electromagnetic waves (> 300 MHz) can be achieved through the utilization of materials with high electrical conductivity. Effective shielding of both electrical and magnetic components can be achieved using good conductors. However, at frequencies below 30 MHz, reducing the magnetic component becomes challenging and is feasible only using ferromagnetic materials.[7] As a result, conductive structures are employed for electrical field shielding, while ferromagnetic materials are utilized for magnetic shielding.[13] Considering the literature, it is emphasized that spinel-structured ferrites are one of fairly efficient materials for electromagnetic shielding. These materials are capable of absorbing magnetic waves in both the high-frequency and ultra-high-frequency regions as a result of their conductivity and loss of magnetic properties in the frequency range. However, their magnetic characteristics reduce in high frequency regions.[14] Magnetite is a ferrimagnetic iron mineral characterized by the Fe_3O_4 formula within the spinel structure. It is commonly known as Ferro-ferric oxide, indicating that iron has two distinct valence states ($2+$ and $3+$) simultaneously, denoted as $FeO.Fe_2O_3$. The material loses its magnetic properties beyond the temperature of 858 K. At room temperature, electrons in magnetite exhibit the property of switching between Fe^{2+} and Fe^{3+} ions. This property categorizes magnetite as a semi-metallic material.[15] Various divalent transition metals such as Co^{2+}, Cu^{2+}, Ni^{2+}, Sn^{2+} etc. can be doped by replacing Fe^{2+} ion in the spinel ferrite structure (MFe_2O_4) to gain different magnetic, catalytic and shielding properties. Specifically, spinel ferrite structure magnetic nano metal oxides, in which Fe^{2+} ions are replaced by M^{2+} ions (M: Co, Ni, etc.), have been developed through various methods, and their ability to inhibit electromagnetic waves has been evaluated.[10c,16] Furthermore, several studies have investigated the shielding properties of composites that contain these particles when applied to materials such as textiles and wood.[5c,10b] Overall, these findings demonstrate the potential of spinel ferrite nanoparticles for enhancing the properties of materials and inhibiting electromagnetic waves in various applications. Studies have also explored the synthesis of nanomagnetic (Fe_3O_4) particles for lower frequencies.[17]

EM shielding paints employ one or several combinations of metallic conductive materials such as nickel (Ni), copper (Cu),

silver (Ag), graphite etc. in order to effectively shield against electromagnetic radiation. Although silver is known as a very effective material for shielding, its high cost is considered a disadvantage. The most commonly used composite paint contains Ni–Cu powder (flakes) and is typically utilized as a primer due to its gray or black colour. Due to its high metal content, it primarily reflects electromagnetic waves.[8a]

Carbon nanotubes (CNTs) have been utilized for electromagnetic (EM) shielding by incorporating them into various materials. To improve the shielding properties, CNT- $CoFe_2O_4$ was added to the electrospun PAN fibers, resulting in a shielding efficiency of approximately 4 dB within the 8–12 GHz frequency range.[18] In another study, the EM shielding effectiveness of a composite material consisting of MWCNT- Fe_3O_4-Fe (MWCNTs with Fe_3O_4 and Fe) was evaluated in the epoxy matrix within the frequency range of 13–40 GHz, and the results showed a range of 40–100 dB.[19] Composite materials were also produced by the blending of silicon carbide (SC), graphene oxide (GO), and epoxide and their electromagnetic (EM) shielding effectiveness were measured within the 8–12 GHz frequency range. The results showed these composites to exhibit shielding effectiveness up to 35–60 dB.[20] Graphene, graphene oxide and carbon nanotubes are among the preferred matrices in the composites for shielding electromagnetic waves because of their advantages in electrical conductivity.

The present study addresses a significant gap in existing literature by providing the first comprehensive investigation into the electromagnetic shielding properties of the MFe_2O_4-PEG-MWCNT mixture in the frequency range of 3.5–12.5 GHz. Additionally, it explores the development of electromagnetic (EM) shielding paints. The primary objective is to synthesize magnetic nanometal oxides with a spinel ferrite structure, MFe_2O_4, (Fe, Co, Sn) and examine their EM shielding properties to advance the development of paints using these nanoparticles for protection against electromagnetic radiation. To achieve this, magnetic nanoparticles (MFe_2O_4) having a spinel ferrite structure (M: Fe, Co, Sn, etc.) were synthesized using the co-precipitation method. Their structural, morphological, and magnetic properties were characterized through FTIR, XRD, TEM, and VSM measurements. The resulting magnetic metal oxide nanoparticles' electromagnetic radiation shielding efficacy was assessed by preparing composite materials with PEG and various conductive materials, including carbon black (cb), multi-walled carbon nanotubes (mwcnt), graphene oxide (go), graphene (gr), and boron carbide (bc), with varying thicknesses and concentrations. The magnetic nanocomposites, demonstrating the highest EM shielding properties, were then incorporated into a water-based wall paint, and their EM efficacy was evaluated.

Results and Discussion

Synthesis and characterization of magnetic MFe_2O_4 (M: Fe^{2+},Co^{2+},Sn^{2+}) nanoparticles

Magnetic MFe_2O_4 (M: Fe^{2+}, Co^{2+}, Sn^{2+}) nanoparticles with a spinel ferrite structure were synthesized through co-precipitation a well-known method recognized for its reproducibility and homogeneous particle size distribution, without producing hazardous by-products. The structural and morphological properties of the synthesized magnetic nanoparticles were characterized using FTIR, TEM, and XRD measurements while their magnetic properties were analysed using VSM measurements.

Fourier transform infrared (FTIR) spectra of the synthesized magnetic nanoparticles are comparatively presented in Figure 1. Spinel ferrite structures (MFe_2O_4) have tetrahedral and octahedral sites hosting cations. Depending on how M^{2+} and Fe^{3+} ions occupy the sites, there are three types of spinel structures: *i)* normal spinel, *ii)* inverse spinel, and *iii)* mixed spinel. In the typical spinel ferrite structure, M^{2+} and Fe^{3+} ions occupy tetrahedral and octahedral sites. However, in inverse spinel ferrite structures, only iron(III) ions occupy the tetrahedral sites in the crystal lattice, while the octahedral sites are randomly shared by metal(II) and iron(III) ions..[21]

The infrared (IR) spectrum of the magnetic nanoparticle crystal lattice in the spinel ferrite structure reveals the bond vibrations of the ions in the range of 350–1000 cm^{-1}.[22] Typically, two characteristic vibration bands of the metal-oxygen bond (M–O) are observed in the FT-IR spectrum based on the bond length. The first occurs at approximately 350–500 cm^{-1}, which is attributed to longer M^{2+}-O and Fe^{3+}-O bonds octahedrally coordinated in the structure. The second occurs in the range of 550–580 cm^{-1} and may be attributed to tetrahedrally coordinated Fe^{3+}-O bonds.[21c] in Figure 1, the peak at 553 cm^{-1} corresponds to the stretching vibrations of Fe^{3+}-O in tetrahedral sites of the structure of Fe_3O_4 nanoparticles. The peak at 440 cm^{-1} corresponds to Fe–O stretching vibrations octahedrally coordinated in the crystal lattice.[21] The shoulder between 600–650 cm^{-1} is most likely attributed to

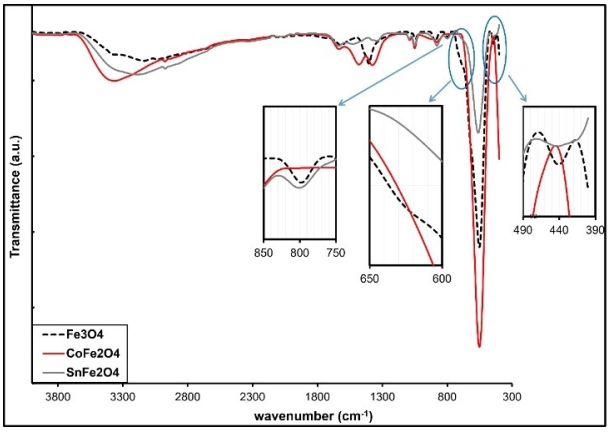

Figure 1. FTIR spectra of the synthesized MFe_2O_4 nanoparticles.

Fe^{2+}-O stretching vibrations which disappeared when Fe^{2+} ions were replaced by Co^{2+} and Sn^{2+} ions in the crystal lattice (*cf.* Figure 1). The stretching vibrations of Fe^{3+}-O bonds in the tetrahedral sites of $CoFe_2O_4$ nanoparticles were observed at the exact wavenumber of 553 cm^{-1}, similar to those observed in Fe_3O_4 nanoparticles. This indicates that $CoFe_2O_4$ nanoparticles probably possess the same inverse spinel structure since the ionic radii of Fe^{2+} and Co^{2+} ions are close to each other. However, the corresponding Fe^{3+}-O vibration peaks in tetrahedral sites were slightly shifted to a higher wavenumber of 561 cm^{-1} with a lower shoulder at 600–650 cm^{-1}. This may be attributed to two reasons: i) the longer ionic radius of Sn^{2+} ions possibly forcing the Fe^{3+}-O bonds to be shorter in the structure, and, ii) $SnFe_2O_4$ nanoparticles potentially having a mixed spinel ferrite structure where Sn^{2+} ions may occupy some tetrahedral sites, as reported in previous studies.[21c,23] Shokri et al. (2018) have identified three bands in the range of 720–880 cm^{-1} in addition to the primary peak at 550–580 cm^{-1}, arising from Fe^{3+}-O vibrations at tetrahedral sites.[21c] These bands could be attributed to Sn^{2+}-O and Fe^{3+}-O vibrations at tetrahedral sites of a mixed spinel ferrite structure. The highest peak at approximately 875 cm^{-1}, together with the primary Fe^{3+}-O bond vibrations in tetrahedral sites, suggest that the other two bands may have originated from a combination of Sn^{2+}-O and Fe^{3+}-O bond vibrations in tetrahedral sites. Consequently, the peaks at 561 and 878 cm^{-1} in Figure 1 could be attributed to the primary Fe^{3+}-O bond vibrations in tetrahedral sites in $SnFe_2O_4$. However, the peak at 800 cm^{-1} indicates the presence of a fraction of Sn^{2+}-O ions occupying tetrahedral sites. No such peak at approximately 800 cm^{-1} is observed for $CoFe_2O_4$ nanoparticles (see Figure 1). The stretching vibrations of Sn^{2+}-O and Fe^{3+}-O in octahedral sites are observed as broad between 400–460 cm^{-1}, while Co^{2+}-O stretching vibrations are observed below 400 cm^{-1}. Furthermore, the O–H stretching vibrations for Fe_3O_4, $CoFe_2O_4$, and $SnFe_2O_4$ were observed at 3175, 3365, and 3168 cm^{-1}, respectively, and their corresponding bending vibrations of O–H bonds on the surface of the nanoparticles were observed at 1620, 1634, and 1640 cm^{-1}.[21c,24]

The size and morphology of the synthesized MFe_2O_4 nanoparticles (M: Fe, Co, and Sn) were characterized using transmission electron microscopy (TEM). The resulting TEM images are given in Figure 2(A), 2(B) and 2(C). It can be observed that the MFe_2O_4 nanoparticles have a uniform particle size distribution and cubic morphology. The average particle sizes were determined to be 10 ± 1, 15 ± 5, and 95 ± 10 nm for Fe_3O_4, $CoFe_2O_4$, and $SnFe_2O_4$ nanoparticles, respectively (*see* Figures 2A–C and Figure S1). The X-ray diffraction (XRD) analysis was performed to investigate crystal structures of MFe_2O_4 nanoparticles. The obtained XRD patterns of the synthesized nanoparticles is given comparatively in Figure 2(D). The prominent diffraction peaks at 2θ values of 30.30°, 35.68°, 37.36°, 43.29°, 53.73°, 57.37°, and 62.88° were indexed to the (220), (311), (400), (422), (511) and (440) planes of the cubic magnetic Fe_3O_4 nanoparticles having an inverse spinel ferrite structure with space group fd-3 m based on international powder diffraction standards (JCPDS Cardno.19–0629).[25] Considering the diffraction patterns from $CoFe_2O_4$ and $SnFe_2O_4$ nanoparticles in Figure 2(D), it is apparent that both $CoFe_2O_4$ and $SnFe_2O_4$ nanoparticles possess an inverse cubic spinel ferrite structure with space group fd-3 m.[25b,26] The X-ray diffraction pattern shown in Figure 2(D) for $CoFe_2O_4$ nanoparticles displays the peaks at 2θ values of 18.61°, 30.4°, 35.75°, 37.46°, 43.40°, 53.91°, 57.29°, 62.86°, 71.33° and 74.20° which can be assigned to reflections from the planes (111), (220), (311), (222), (400), (422), (511), (440), (622), and (533), respectively, in the inverse cubic spinel ferrite structure with space group fd-3 m (JCPDS Cardno.22–1086).[25b,26] Although the peaks in the XRD pattern for $SnFe_2O_4$ nanoparticles were observed at lower 2θ values

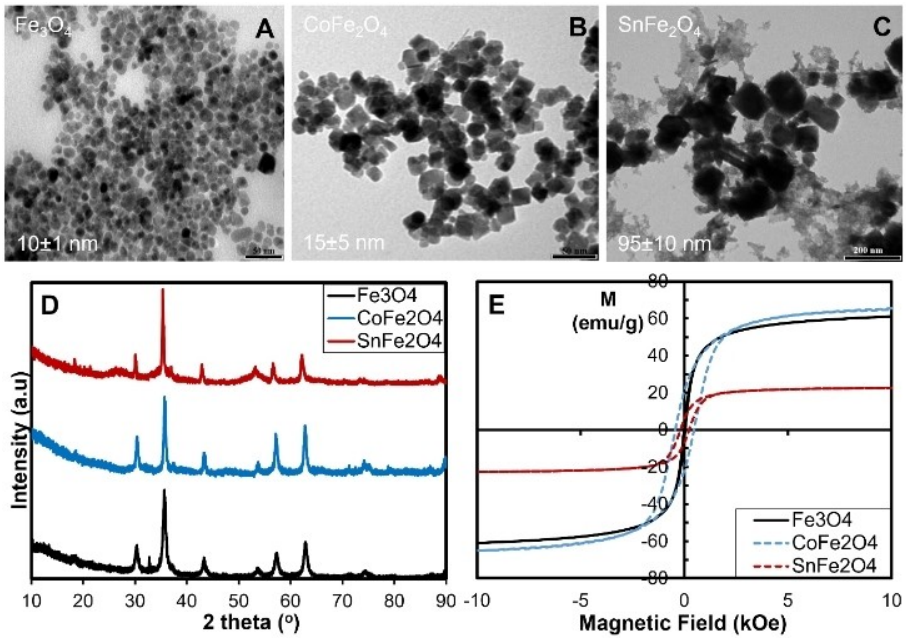

Figure 2. Characterization data from TEM (A–C), XRD (D), and VSM (E) measurements of the synthesized MFe_2O_4 nanoparticles.

compared to those of $CoFe_2O_4$ nanoparticles, the peaks were also indexed to reflections from the (111), (220), (311), (222), (400), (422), (511) and (440) planes of $SnFe_2O_4$ indicating an inverse cubic spinel ferrite structure with space group fd-3 m (JCPDS Cardno.10–0325).[25b,27] The corresponding 2θ values are consistent with the reported data for $SnFe_2O_4$ nanoparticles.[27a]

The magnetic properties of the synthesized MFe_2O_4 nanoparticles were determined using a vibrating sample magnetometer (VSM) by applying an external magnetic field in the ±10 kOe range at room temperature. The resulting plots of magnetization (emu/g) as a function of magnetic field (Oe) are given in Figure 2E. The synthesized magnetic Fe_3O_4 nanoparticles exhibit superparamagnetism as evidenced by the absence of a hysteresis loop in Figure 2E,[28] and possess a saturation magnetization (Ms) value of approximately 61 emu/g. However, $CoFe_2O_4$ and $SnFe_2O_4$ nanoparticles demonstrate soft ferromagnetic characteristics with relatively narrow hysteresis loops.[28a] The saturation magnetization of $CoFe_2O_4$ was determined to be 65 emu/g, whereas the magnetization was 22.7 emu/g for larger $SnFe_2O_4$ nanoparticles with 95 nm. Other magnetic characteristics of the $CoFe_2O_4$ and $SnFe_2O_4$ nanoparticles were investigated by analysing various magnetic parameters, including the remanent magnetization (Mr), coercivity (Hc), and remanence ratio (Mr/Ms). These parameters were obtained by analysing the magnetization (emu/g) versus magnetic field (Oe) plots and determining the corresponding intercepts on the x- and y-axes, respectively. The obtained values for the various magnetic parameters are presented in Table 1.

The coercivity values of the $CoFe_2O_4$ and $SnFe_2O_4$ nanoparticles were determined to be 454 and 210 Oe, respectively. The coercivity of magnetic materials is a measure that signifies the strength of the magnetic field required to reduce its magnetization to zero, subsequent to reaching saturation.[26b,28a] This property is highly dependent on the size of the material in question. As the size of particles decreases, the coercivity initially increases until it reaches a maximum and then begins to decrease toward zero. Once the critical diameter is reached, the coercivity becomes zero. At this point, the particles have a single domain structure, and they transition to a superparamagnetic structure.[26b,28a] The coercivity of $CoFe_2O_4$ nanoparticles is found to be lower than what has been reported in previous studies.[26a,29] This value falls within the expected limits for nanoparticles with a size of 15 nm, as stated in the literature.[26a] On the other hand, the magnetic saturation (Ms) of $SnFe_2O_4$ nanoparticles is lower, and as a result, the coercivity is larger than what has been reported in the literature since the particles were synthesized with a larger size..[21c,26a,30] The remanence ratios of the $CoFe_2O_4$ and $SnFe_2O_4$ nanoparticles were determined to be 0.33 and 0.28, respectively. These values suggest that the particles have a single domain structure since the Mr/Ms ratio < 0.5.[26a,31]

Table 1. Magnetic properties of the synthesized MFe_2O_4 nanoparticles (Ms: saturation magnetization; Mr: remanent magnetization and Mr/Ms: remanence ratio).

MFe_2O_4	Size (nm)	Ms (emu/g)	Mr (emu/g)	coercivity (Oe)	Mr/Ms
Fe_3O_4	10±1	61	–	–	–
$CoFe_2O_4$	15±5	65	21.5	454	0.33
$SnFe_2O_4$	95±10	23	6.5	210	0.28

Electromagnetic shielding measurements

Selection of coating substrate

Glass, cardboard and cellulose acetate films were used to choose a suitable substrate for electromagnetic (EM) measurements. The selected substrate should not exhibit either absorption or reflection in the working EM frequency range. The first optimization studies aimed to compare the effect of substrate type on electromagnetic (EM) shielding. Aqueous dispersions containing MFe_2O_4:PEG (1:5) were mixed with commercial water-based paint in a 1:1 weight ratio, and the resulting mixture was applied to a glass surface using dipping and thin film methods. The EM shielding results for the 3.3–7.05 GHz range are presented in Tables S1 and S2 (see *Supporting Information*). The EM shielding results showed that magnetic Fe_3O_4 nanoparticles-paint mixture on the glass surface provided up to 50% shielding at some frequencies on glass substrates. However, it should be noted that the observed results are attributable to the glass and its composition. In studies on electromagnetic (EM) shielding, it is essential for materials to exhibit minimal reflection to avoid becoming a new source of EM waves in the surrounding environment. As such, glass substrates were deemed unsuitable due to their inherent higher reflection and absorption properties within the operational range of EM radiation, as illustrated in Figure S2. To reduce the absorption and reflection of electromagnetic (EM) waves, cardboard surfaces of equivalent size and thickness to the glass substrate were employed as substrates. However, the cardboard substrate experienced deformation upon wetting, resulting in markedly low shielding efficiencies. On the other hand, the paint used in the experiment exhibited some inherent EM shielding properties due to its composition, thereby making it difficult for isolation of the EM shielding properties of the MFe_2O_4 nanoparticles. As a result, subsequent optimization measurements were conducted exclusively on coatings containing aqueous dispersions of MFe_2O_4 nanoparticles, applied onto acetate film surfaces (see Table S3). The frequency range under investigation for shielding efficiency was changed to the range of 8.2–12.5 GHz, which aligns with the higher shielding capabilities of the magnetic nanoparticles, and acetate paper sheets were selected as the substrate material. Various parameters, including the conductive material, ratio, and coating thickness, were systematically tested in the coatings comprising solely of aqueous MFe_2O_4 nanoparticle dispersions, to achieve significant shielding efficiency. (See Table S2).

Effect of conductive material type and amount

The electromagnetic shielding performance is enhanced by the conductivity and magnetic properties of the material, with conductivity being a crucial parameter.[32] Initial studies using mixtures containing only magnetic Fe_3O_4 nanoparticles did not achieve the desired shielding performance within the specified thickness range. To enhance the electromagnetic shielding properties, various conductive materials, such as carbon black (cb), multi-walled carbon nanotubes (mwcnt), graphene oxide (go), graphene (gr), and boron carbide (bc), were added to aqueous dispersions of Fe_3O_4:PEG nanoparticles (1:5). Conductive materials were added and dispersed in a weight ratio of 50:1 at 10,000 rpm for 15 minutes. Subsequently, the dispersions were coated onto a 120-micron thick cellulose acetate sheet using the thin film method. Electromagnetic shielding measurements were performed in the X-band frequency range of 8.2–12.5 GHz, and the results are presented in Table S3 and Figure 3(A). The samples containing multiwalled carbon nanotubes (mwcnt) exhibited the most significant improvement in electromagnetic shielding performance. The study revealed that the shielding effectiveness of the material was significantly improved to approximately 40% from its original value of around 20% by increasing the amount of the mwcnts in the mixture by a factor of five, as shown in Table S3 and Figure 3(A).

Furthermore, it was observed that the acetate sheet substrate had negligible electromagnetic (EM) shielding properties as seen by the gray dashed line in Figure 3(B). Subsequently, the influence of varying mwcnt amounts on the EM shielding performance of the Fe_3O_4:PEG mixture was investigated in the frequency range of 8.2–12.5 GHz, with mwcnts identified as a more effective conductive material for EM shielding. Three different ratios of [Fe_3O_4:PEG]:mwcnt, namely 50:1, 50:5, and 50:10, were prepared in an aqueous solution and coated on acetate sheets using the thin film coating method. The EM shielding properties were measured in the range of 8.2–12.5 GHz. The results revealed that the EM shielding effectiveness increased with increasing the amounts of multiwalled carbon nanotubes (mwcnts) in the aqueous Fe_3O_4:PEG mixture (see Table S3 and Figure 3(B)). Based on the observed improvements, the study ratio of [Fe_3O_4:PEG]:mwcnt ratio of 50:10 was selected as the optimal ratio for further study. The decision to use this ratio was based on the most significant enhancement in EM shielding properties.

Effect of sample thickness

The influence of coating thickness on the electromagnetic (EM) shielding performance was investigated through a comparative analysis of two types of coated samples: Fe_3O_4:PEG and [Fe_3O_4:PEG]:mwcnt mixtures in the range of 8.2–12.5 GHz. The magnetic material compositions used in these experiments were kept constant at a ratio of 1:1 for the aqueous Fe_3O_4:PEG mixture and 50:10 for [Fe_3O_4:PEG]:mwcnt. A standard EM shielding test was applied on acetate sheets measuring 1x1 cm, coated with a thickness of 120 microns using the thin film method. To investigate the impact of coating thickness, EM shielding measurements were conducted on the two, four, and six overlayed coated samples with corresponding thicknesses of 240, 480, and 720 microns, respectively. The findings revealed that the EM shielding properties of samples coated solely with magnetic nanoparticles increased with increasing coating thickness. Notably, a shielding efficiency of 2.5 dB was achieved with six overlayed acetate sheets coated with a Fe_3O_4:PEG mixture (~720-micron thickness), resulting in 25% shielding of EM waves. On the other hand, when the conductive material (mwcnt) was incorporated into the magnetic material (Fe_3O_4:PEG) at a ratio of 10:50, the shielding efficiency was measured as 17 dB for a 120-micron thick coating. Remarkably, a shielding efficiency of 52 dB was attained by further increasing the coating thickness to ~720 microns with six overlayed coated samples in the frequency range of 8.2–12.5 GHz (see Table 2, Figure 3(C)) The comparative graphs were given in Figure S3 to show the effect of coating thickness on EM shielding properties of all MFe_2O_4 nanoparticles. (*see Supporting Information*)

Consequently, the optimization study revealed that the shielding efficiency of magnetic nanoparticles can be enhanced by incorporating a conductive material, increasing the amount of conductive material and coating thickness. These findings are consistent with the results reported by Mostaani et al. (2018).[32] Based on the optimization study, it was determined that multiwalled carbon nanotubes are better as conductive

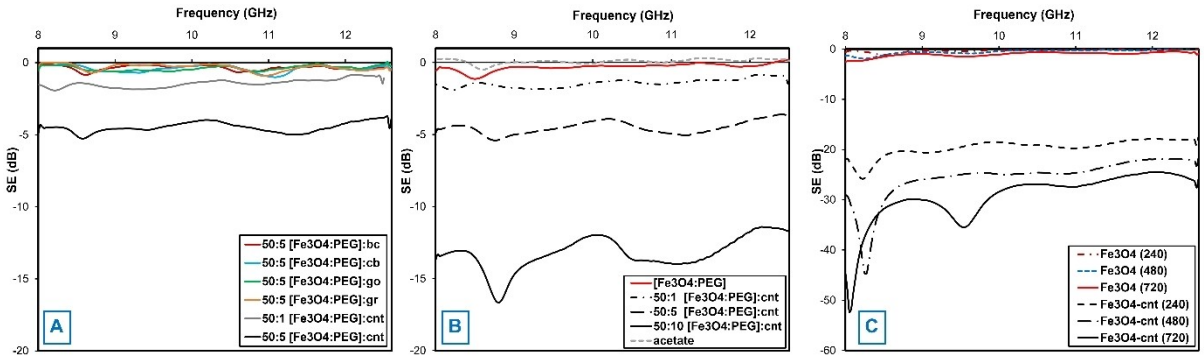

Figure 3. Effect of the conductive material (A), amount of conductive material (B) and coating thickness (C) on the electromagnetic shielding properties (*abbr.* bc: boron carbide, cb: carbon black, go: graphene oxide, gr: graphite, cnt: multiwalled carbon nanotube.

Table 2. Electromagnetic shielding performance of Fe_3O_4 and Fe_3O_4-mwcnt depending on the coating thickness and conductive material amount in the range of 8.2–12.5 GHz.

Code	t (μm)[a]	Material composition	SE (dB)	% shielding
Effect of conductive materials amount				
[Fe_3O_4:PEG]	120	[Fe_3O_4:PEG] (1:1)	0.0–0.8	0.0–9.0
50:1 [Fe_3O_4:PEG]:cnt	120	50:1 [Fe_3O_4:PEG]:mwcnt	1.5–2.5	15.9–25.0
50:5 [Fe_3O_4:PEG]:cnt	120	50:5 [Fe_3O_4:PEG]:mwcnt	3.8–5.3	35.0–44.0
50:10 [Fe_3O_4:PEG]:cnt	120	50:10 [Fe_3O_4:PEG]:mwcnt	12.0–17.0	75.0–85.9
Effect of coating thickness				
Fe_3O_4 (240)	240	[Fe_3O_4:PEG] (1:1)	0.0–1.5	0.0–15.9
Fe_3O_4 (480)	480	[Fe_3O_4:PEG] (1:1)	0.8–2.0	9.0–20.6
Fe_3O_4 (720)	720	[Fe_3O_4:PEG] (1:1)	0.0–2.5	0.0–25.0
Fe_3O_4-cnt (240)	240	50:10 [Fe_3O_4:PEG]:mwcnt	18.0–25.0	87.4–94.4
Fe_3O_4-cnt (480)	480	50:10 [Fe_3O_4:PEG]:mwcnt	22.0–45.0	92.1–99.4
Fe_3O_4-cnt (720)	720	50:10 [Fe_3O_4:PEG]:mwcnt	24.5–52.0	94.0–99.8
Acetate	–	Uncoated	0	0

[a] t: coating thickness.

materials, and the optimal ratio of [MFe_2O_4:PEG]:mwcnt in aqueous mixtures is 50:10.

Electromagnetic shielding properties of different magnetic MFe_2O_4 (M:Fe^{2+}, Co^{2+}, Sn^{2+}) nanoparticles in the range of 8.2–12.5 GHz

The electromagnetic (EM) shielding properties of three different spinel ferrite nanoparticles, namely MFe_2O_4 (M: Fe^{2+}, Co^{2+}, Sn^{2+}), were comparatively investigated in the frequency range of 8.2–12.5 GHz. The EM shielding capabilities of both the bare MFe_2O_4 nanoparticles and mixtures of MFe_2O_4 with multi-walled carbon nanotubes were systematically measured, taking into account the conductive material composition and coating thickness. The results revealed that the EM shielding performance of bare MFe_2O_4 nanoparticles (where M=Fe^{2+}, Co^{2+}, Sn^{2+}) with a thickness of 240 microns in the frequency range of 8.2–12.5 GHz was relatively low, with the shielding efficiency values of 1.5, 0.6, and 1.5 dB, respectively. However, the shielding efficiency improved by approximately two-fold when the coating thickness was increased from 240 microns to 720 microns, as shown in Figure S2 and Table S4. The EM shielding efficiencies of bare MFe_2O_4 nanoparticles with a coating thickness of ~720 microns were measured on six overlayed samples, resulting in shielding efficiency values of 2.5, 1.2, and 3.0 dB for Fe_3O_4, $CoFe_2O_4$ and $SnFe_2O_4$ nanoparticles, respectively. The corresponding results show that MFe_2O_4 nanoparticles can shield up to 25%, 13%, and 29% of EM radiation in the frequency range of 8.2–12.5 GHz, respectively and higher shielding effectiveness can be achieved by increasing the coating thickness containing bare MFe_2O_4 nanoparticles, as seen in Figure 4.

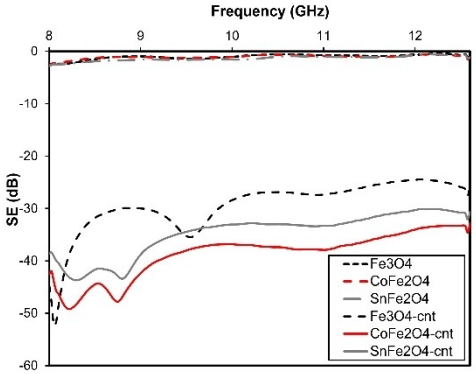

Code	Thickness	Sample	SE (dB) (max.-min.)	% shielding
Fe_3O_4	720 μm	[Fe_3O_4:PEG]	0.0–2.5	0.0–25.0
$CoFe_2O_4$	720 μm	[$CoFe_2O_4$:PEG]	0.0–1.2	0.0–13.0
$SnFe_2O_4$	720 μm	[$SnFe_2O_4$:PEG]	0.8–3.0	9.0–29.0
Fe_3O_4-cnt	720 μm	[Fe_3O_4:PEG]:mwcnt 50:10	24.5-52.0	94.0-99.8
$CoFe_2O_4$-cnt	720 μm	[$CoFe_2O_4$:PEG]:mwcnt 50:10	34.0-49.0	98.0-99.6
$SnFe_2O_4$-cnt	720 μm	[$SnFe_2O_4$:PEG]:mwcnt 50:10	30.0-44.0	96.9-99.4

Figure 4. Electromagnetic shielding measurements of different magnetic MFe_2O_4 (M:Fe^{2+},Co^{2+},Sn^{2+}) nanoparticles between 8.2–12.5 GHz.

Change in the electromagnetic shielding properties of magnetic MFe_2O_4 ($M:Fe^{2+},Co^{2+},Sn^{2+}$) nanoparticles depending on the frequency of EM radiation

Following the assessment of the electromagnetic (EM) shielding performance of MFe_2O_4 (M: Fe^{2+}, Co^{2+}, Sn^{2+}) nanoparticles in the X-band range, further studies were carried out for investigation of their performances in the lower frequency ranges of 5.5–8.5 GHz and 3.5–6.0 GHz, respectively. Specifically, only samples coated with a 50:10 ratio of [MFe_2O_4:PEG]:mwcnt mixtures, 240 microns thick, were compared within the 5.8–8.2 GHz range (see Figure 5). The results were found to be in agreement with those obtained in the X-band range, and no significant differences were observed in the effects of the various magnetic nanoparticles on EM shielding at lower frequencies. Shielding efficiency of up to 94% was achieved with only two overlayed samples coated with a mixture of [MFe_2O_4:PEG]:mwcnt in a ratio of 50:10 (as shown in Figure 5). It was observed that the shielding efficiency varied by the order $CoFe_2O_4 > Fe_3O_4 > SnFe_2O_4$. The shielding values obtained for a thickness of ~240 microns were higher at lower frequencies than those obtained for the frequency range of 8.2–12.5 GHz. Therefore, it can be concluded that the shielding performance of MFe_2O_4 nanoparticles is better at lower frequencies.

The shielding data in this study are comparatively summarized with the literature in Table 3. In order to ensure a suitable comparison, the materials with relatively thinner coatings were selected from the literature. Only the highest results in each frequency range from this study were given in Table 3. Considering the results presented in Table 3, it can be concluded that the highest electromagnetic shielding properties in this study were comparable to the data from the literature even though they were obtained with thinner coatings (see Table 3). The addition of conductive materials and/or increasing the thickness of the coatings will further improve the shielding efficiency. On the other hand, the magnetic nanoparticle type and the measured frequency range do not much affect the electromagnetic shielding properties of the surface coating since there is no systematic differences between the shielding efficiencies obtained from different magnetic nanoparticles (*cf.* Figures 4 and 5).

EM Shielding Properties of Paint Samples Containing Magnetic MFe_2O_4 Nanoparticles

The electromagnetic shielding properties of wall paint-magnetic, MFe_2O_4 (M: Fe^{2+}, Co^{2+}, Sn^{2+}) nanoparticle composites were investigated in the range of 8.2–12.5 GHz. A mixture of magnetic MFe_2O_4:mwcnt (50:10) and water-soluble wall paint with a 1:2 weight ratio was prepared to analyse whether the inclusion of MFe_2O_4:mwcnt (50:10) materials in standard water-soluble wall paint could enhance its EM shielding capabilities in comparison to conventional paint (dyes). The mixture was homogenized by a homogenizer at 10000 rpm for 15 min and then coated on acetate paper sheets with 120 microns. The EM

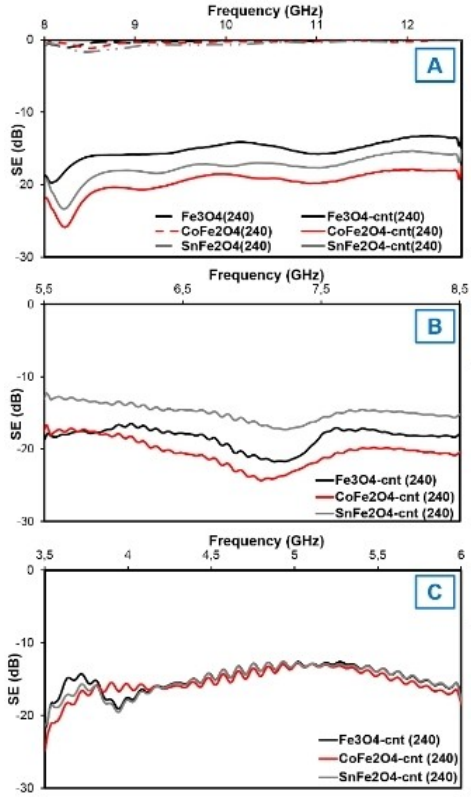

Frequency range: 8.2–12.5 GHz

Code	Thickness	Sample	SE (dB) (max.min.)	% shielding
Fe_3O_4-cnt	240 μm	[Fe_3O_4:PEG]:cnt 50:10	18–25	87.4–94.4
$CoFe_2O_4$-cnt	240 μm	[$CoFe_2O_4$:PEG]:cnt 50:10	11–19	71.8–88.3
$SnFe_2O_4$-cnt	240 μm	[$SnFe_2O_4$:PEG]:cnt 50:10	15–24	82.2–93.7

Frequency range: 5.5–8.5 GHz

Code	Thickness	Sample	SE (dB) (max.min.)	% shielding
Fe_3O_4-cnt	240 μm	[Fe_3O_4:PEG]:cnt 50:10	13–17	77.6–85.9
$CoFe_2O_4$-cnt	240 μm	[$CoFe_2O_4$:PEG]:cnt 50:10	17–24	85.9–93.7
$SnFe_2O_4$-cnt	240 μm	[$SnFe_2O_4$:PEG]:cnt 50:10	17–22	85.9–92.1

Frequency range: 3.5–6.0 GHz

Code	Thickness	Sample	SE (dB) (max.min.)	% shielding
Fe_3O_4-cnt	240 μm	[Fe_3O_4:PEG]:cnt 50:10	12–20	74.9–90.0
$CoFe_2O_4$-cnt	240 μm	[$CoFe_2O_4$:PEG]:cnt 50:10	13–23	77.6–92.9
$SnFe_2O_4$-cnt	240 μm	[$SnFe_2O_4$:PEG]:cnt 50:10	13–20	77.6–90.0

Figure 5. Electromagnetic shielding measurements of different magnetic MFe_2O_4 ($M:Fe^{2+},Co^{2+},Sn^{2+}$) nanoparticles in the frequency range of 8.2–12.5 (A), 5.5–8.5 (B) and 3.5–6.0 (C) GHz.

Table 3. Comparison of the EM shielding values of the obtained coating materials with those in the literature.

Nanoparticle-composite system	Thickness (mm)	Frequency range (GHz)	Shielding (dB)	Literature
[$CoFe_2O_4$:PEG]:mwcnt (50:10)	0.24	3.5–6.0	23	This study
[$CoFe_2O_4$:PEG]:mwcnt (50:10)	0.24	5.5–8.5	24	This study
[Fe_3O_4:PEG]:mwcnt (50:10)	0.24	8.2–12.5	25	This study
[Fe_3O_4:PEG]:mwcnt (50:10)	0.72	8.2–12.5	52	This study
%15 Fe_3O_4/%50 Carbon Black (cb)	0.7	8.2–12.4	36.6	[33]
PANI/% 20 Nb_2O_5	–	8–12	28.8	[34]
Ultrahigh performance concrete (UHPC)/%2 cnt)	3	0,1–1.5	25	[35]
PMMA/10 wt% MLG/10 wt% MWCNT	2	8–12	43	[36]
3D CNT-Epoxy	5	8–12	55	[20b]
CNT-GO-PMMA	16	2–18	60	[20d]
Cement-stainless steel powder	5	0.5–1.5	6–9	[37]
Ti_3AlC_2 doped ceramic	23	12–18	40	[38]
$CoFe_2O_4$–ZnS–GO	5	2–18	43	[16a]
Wood-$BaSO_4$–C–Fe_2O_3–$NiSO_4$	10	0.3–2.4	52	[39]
$CoFe_2O_4$–SnS_2–GO	1.6	8–12	54	[10c]
PS–Fe_2O_4–GO	–	8–12	30	[12b]
PANI-$BaTiO_3$	3	12–18	70	[40]
$CoFe_2O_4$–cnt–PAN	1	12–18	4	[18]
$Ni_{0.5}Zn_{0.5}Fe_2O_4$/MWCNTs	1.2	8.2–12.4	40.1	[41]

shielding efficiencies measurements were performed on six overlayed samples in the 8.2–12.5 GHz frequency range. Considering the results in Figure 6, it was observed that the paint exhibited shielding behaviour at a specific ratio, which is consistent with expectations due to the shielding property of TiO_2 in the white wall paint within the frequency range of the study.[38,40] However, the samples containing MFe_2O_4-mwcnt nanoparticles showed a significant improvement in EM radiation shielding within the working frequency range. The highest EM shielding efficiency was measured for the samples coated with paint mixtures containing $CoFe_2O_4$:mwcnt, while the coatings with $SnFe_2O_4$-mwcnt:paint mixtures demonstrated the lowest shielding properties. Comparing the EM shielding results in Figure 6 with measurements from MFe2O4:mwcnt samples of the same thickness within the 8.2–12.5 GHz frequency range (see Figure 4), it can be observed that the paint somewhat reduced the EM shielding efficiencies of the samples by approximately one-third. This reduction can be attributed to the dilution of MFe_2O_4 with paint, as the sample was prepared by mixing the optimized MFe_2O_4:mwcnt (50:10) sample for its EM shielding property with paint at a 1:2 weight ratio. The best shielding results in the paint-containing samples were observed in the samples coated by [$SnFe_2O_4$:mwcnt]:paint with the shielding percentage of 84% within the 8.2–12.5 GHz range. Changes in the characteristic properties of paints with the addition of magnetic materials were investigated through standard light transmittance and hardness tests. To this end, paint mixtures were prepared and coated on a 3x3 cm glass

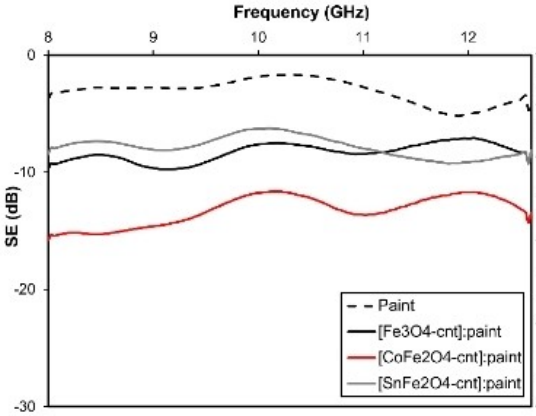

Code	Thickness	SE (dB) (max.-min.)	% shielding
Paint	720 μm	1.8-5.0	18.7-43.8
[Fe_3O_4-cnt]:paint	720 μm	7.0-10	55.3-68.4
[$CoFe_2O_4$-cnt]:paint	720 μm	6.2-9.0	51.0-64.5
[$SnFe_2O_4$-cnt]:paint	720 μm	11.7-16	74.0-84.2

Figure 6. Electromagnetic shielding measurements of wall paint-magnetic nanoparticle mixtures between 8.2–12.5 GHz.

surface using the thin film method with a thickness of 120 microns. The light transmittance of the samples was measured at a wavelength of 550 nm using a Haze-gard plus device. The pencil hardness method was employed using pencils with hardness ranging from 9H to 8B to evaluate the mechanical strength of the coatings. The results showed a reduction in the light tolerance of paints with magnetic material addition. Additionally, the coatings obtained with the water-soluble paint (MFe_2O_4:mwcnt) exhibited poor mechanical strength and adhesion problems on the glass surface, indicating a need for improvement.

Conclusions

Shielding electromagnetic radiation is vitally important to protect against possible adverse effects on human health. For this aim, we present the synthesis of three types of spinel ferrite nanoparticles, namely Fe_3O_4, $CoFe_2O_4$, and $SnFe_2O_4$, and employ them to develop electromagnetic shielding paints. Magnetic nanoparticles, including Fe_3O_4, $CoFe_2O_4$, and $SnFe_2O_4$, with sizes of 10 ± 1, 15 ± 5, and 95 ± 20 nm, respectively, were synthesized through the co-precipitation method. The electromagnetic (EM) shielding properties of these nanoparticles and their corresponding factors were subsequently studied. Although magnetic nanoparticles synthesized exhibited lower EM shielding properties, it was observed the shielding efficiency could be increased by increasing the coating thickness and conductivity. Various conductive materials, such as multiwalled carbon nanotube (mwcnt), graphene (gr), graphene oxide (go), carbon black (cb) and boron carbide (bc), were tested, where the most significant improvements were observed in samples with added multiwalled carbon nanotubes (mwcnts). Different ratios of mwcnts were added to the synthesized MFe_2O_4 nanoparticles, and the EM shielding efficiency improved as the mwcnt ratio increased. [Fe_3O_4:PEG]:mwcnt ratios of 50:1, 50:5, and 50:10 were prepared, and the best EM shielding results were achieved with a 50:10 mwcnt ratio in a mixture of [Fe_3O_4:PEG (1:1)]. The best EM shielding efficiency in the range of 3.5–12.5 GHz were achieved as 52 dB with the sample coated by [Fe_3O_4:PEG]:mwcnt (50:10) mixture having 0.72 mm thickness, corresponding to a shielding percentage of 99.75 %. Magnetic MFe_2O_4 nanoparticles with optimum compositions were mixed with a standard water-soluble wall paint at a 1:2 weight ratio, and the resulting EM shielding properties of the paint mixtures containing [Fe_3O_4:PEG]:mwcnt (50:10) ratio achieved 84 % shielding with a coating thickness of 0.72 mm. However, the mechanical properties of the [Fe_3O_4:PEG]:mwcnt (50:10):paint mixture needs improvement. This study presents a comprehensive perspective to protect human beings from possible negative effects of EM radiations inevitably surrounding our environment. The protective paints to be developed using EM shielding materials having absorptive properties against EM radiation pollution can help to increase living quality in closed places in the near future.

Experimental

Materials

Iron(III) chloride hexahydrate ($FeCl_3.6H_2O$, Merck), iron(II) chloride tetrahydrate ($FeCl_2.4H_2O$, Merck), tin(II) chloride dihydrate ($SnCl_2.2H_2O$, Merck), and cobalt(II) chloride hexahydrate ($CoCl_2.6H_2O$, Merck) were used as precursors for the synthesis of nanoparticles. Sodium hydroxide (Merck) and ammonia (35 %, Merck) were used for basic conditions. Polyethylene glycol (PEG 8000, Acros) was used to disperse magnetic nanoparticles, and argon gas (99.9999 %) provided an inert atmosphere. Multiwalled carbon nanotubes (MWCNTs, Nanocyl), graphene (Nanography Company, purity 99.9 %), graphene oxide (Nanography, Purity 99.5 %), and boron carbide (Boroptic 94 %) were used to ensure the conductivity of the medium. Ultrapure water was used in all studies performed in an aqueous medium. All chemicals were used as supplied without further purification.

Synthesis of magnetic MFe_2O_4 (M:Fe^{2+},Co^{2+},Sn^{2+}) nanoparticles

Magnetic nano metal oxide (MFe_2O_4) particles (M: Fe^{2+}, Co^{2+}, Sn^{2+}) were synthesized in an aqueous solution under basic conditions and an argon atmosphere by a coprecipitation method[25a] (Eq. 4). In a typical synthesis, weighed amounts of metal(II) chloride hydrate (M: Fe^{2+}, Co^{2+}, Sn^{2+}) and iron(III) chloride hexahydrate ($FeCl_3.6H_2O$) with a 1:2 molar ratio of M^{2+}:Fe^{3+} were dissolved in 100 mL of argon-washed ultrapure water. The solution was then heated to 90 °C with stirring at 800 rpm, and ammonia solution (32 %) was added dropwise to the solution up to pH 10–11. Then, the blackish mixture was heated at 90 °C for 1 hour under an argon atmosphere. The synthesized magnetic MFe_2O_4 nanoparticles were cooled at room temperature and separated using a magnet. Magnetic MFe_2O_4 was washed with ultrapure water several times to remove excess base residue and then dried at 40 °C in a vacuum oven.

$$M^{2+} + 2Fe^{3+} + 8OH^- \rightarrow MFe_2O_4 + 4H_2O \quad (4)$$

The structural, morphological, and magnetic properties of the magnetic nanoparticles were characterized by Fourier transform infrared spectroscopy (FTIR), X-ray diffraction (XRD), transmission electron microscopy (TEM) and vibrating sample magnetometer (VSM) measurements. FTIR spectrometric measurements were performed by a Perkin Elmer TWO model FTIR spectrometer with the ATR technique. XRD measurements characterized the crystal phases of the magnetic MFe_2O_4 nanoparticles. XRD measurements of the nanoparticles were measured by using a Bruker Axs D8 Advance Model diffractometer operated with Cu Kα radiation in the 2θ range of 0–80° with a scanning rate of 0.01 degrees/s according to the powder diffraction technique. Zeiss Leo 906E TEM instrument was used to determine the size and morphology of magnetic nanoparticles by counting 200 particles in TEM images by the ImageJ program. Measurements were performed at 80 kV using the samples coated on carbon-coated copper grids. The magnetic properties of all synthesized MFe_2O_4 nanoparticles were determined by VSM measurements by applying an external magnetic field at ± 1.0 Tesla range at room temperature. Measurements were performed with a Cryogenic Limited PPMS Vibrating Sample Magnetometer.

Electromagnetic (EM) shielding measurements

Electromagnetic (EM) shielding measurements were carried out using an Anritsu VNA Master MS2028 C model vector network

analyser where test samples were placed inside metallic waveguide structures with suitable geometry at each frequency range. The measurements were performed at three frequency regions between 3.5–12.5 GHz frequencies using WR187 waveguide for 3.5–5.85 GHz, WR137 waveguide for 5.85–8.20 GHz, and WR90 waveguide for 8.2–12.5 GHz. The system was calibrated with the Anritsu OSLN50 A–18 calibration kit prior to measurement with each waveguide. The synthesized magnetic MFe_2O_4 nanoparticles were mixed with polyethylene glycol (8000 g/mol) in 10 mL of ultrapure water to a ratio of 1:5 by weight of PEG: MFe_2O_4 and mixed with a homogenizer for 10 minutes at 10000 rpm. At the end of this period, the mixture was applied on the surfaces of the selected substrates (glass, cardboard, and cellulose acetate film) with a thickness of 120 microns by the thin film coating technique using an Erichsen manual film applicator and dried at room temperature. EM shielding measurements were performed by cutting 3x6 cm and 2.5x2.5 cm dimensions from the dried samples. The effect of parameters such as the coating method (dipping and thin film coating), conductivity, and application substrate (glass, cardboard, and cellulose acetate film) on the EM shielding measurement was optimized. For conductivity, multiwalled carbon nanotubes (MWCNTs), carbon black (CB), graphene (GR), graphene oxide (GO), and boron carbide (BC) were added to the mixture in 50:1 and 50:5 ratios, and their effects on EM shielding were investigated. Then, the EM shielding effects of 50:1, 50:5, and 50:10 by weight of the MWCNT sample with the best shielding effect were investigated with [Fe_3O_4:PEG (1:1)]. According to the results obtained, [MFe_2O_4:PE (1:1)] and MWCNTs were mixed in a 50:10 ratio, and the EM shielding effects were investigated.

Acknowledgements

The authors acknowledge the Akdeniz University Coordination Unit of Scientific Research Projects (project no. FYL-2018-3594) for their financial support. The authors especially thank Department of Electrical and Electronical Engineering, Faculty of Engineering, Akdeniz University and Department of Electrical and Electronical Engineering, Faculty of Engineering, Antalya Bilim University, Antalya, Turkey for permission to use their facilities for EM shielding measurements.

Conflict of Interests

The authors declare no conflict of interest.

Data Availability Statement

The data that support the findings of this study are available from the corresponding author upon reasonable request.

Keywords: electromagnetic shielding · magnetic nanoparticles · paint · spinel ferrites (MFe_2O_4) · X band

[1] N. Gaudin, in *The WHO/International Agency for Research on Cancer (IARC)* **2011**.
[2] A. B. F. Yagmur, I. H. Hancı, *Sürekli Tıp Eğitimi Dergisi (STED)* **2003**, *12*, 296–297.
[3] L. Kheifets, M. Repacholi, R. Saunders, E. van Deventer, *Pediatrics* **2005**, *116*, E303-E313.
[4] G. Lundell, in *Proceedings of the 2004 EPRI-Cosponsored World Health Organization Workshop, Vol. 1011147* (Ed.: G. Lundell), **2004**, p. 1011147.
[5] a) M. C. Ribadeneyra, Ph.D. thesis, Charles III University of Madrid (Leganes, Madrid, Spain), **2014**; b) D. Wanasinghe, F. Aslani, *Compos. B. Eng.* **2019**, *176*, 1–24; c) N. D. Sema Palamutcu, *Tekstil Teknolojileri Elektronik Dergisi* **2009**, *3*, 87–101; d) V. Shukla, *Nanoscale Adv.* **2019**, *1*, 1640–1671.
[6] R. Yılmaz, *Electronic Journal of Vocational Colleges* **2014**, *4*, 136–150.
[7] H. Aniolczyk, J. Koprowska, P. Mamrot, J. Lichawska, *Fibres Text. East. Eur.* **2004**, *12*, 47–50.
[8] a) S. Dagli, *Paintindia* **2011**, *61(2)*, 45–43; b) H. S. Lee, H. B. Choe, I. Y. Baek, J. K. Singh, M. A. Ismail, *Materials* **2017**, *10*, 1–14.
[9] a) S. Geetha, K. K. S. Kumar, C. R. K. Rao, M. Vijayan, D. C. Trivedi, *J. Appl. Polym. Sci.* **2009**, *112*, 2073–2086; b) A. Ameli, M. Nofar, S. Wang, C. B. Park, *ACS Appl. Mater. Interfaces* **2014**, *6*, 11091–11100.
[10] a) İ. K. M. Altun, M. Güneş, M. H. Alma, *KSU Mühendislik Bilimleri Dergisi* **2017**, *20*, 38–47 b) W. T. Gan, Y. Liu, L. K. Gao, X. X. Zhan, J. Li, *Ceram Int* **2015**, *41*, 14876–14885; c) N. Zhang, Y. Huang, M. Zong, X. Ding, S. P. Li, M. Y. Wang, *Ceram. Int.* **2016**, *42*, 18879–18886.a) İ. K. M. Altun, M. Güneş, M.H. Alma, *KSU Mühendislik Bilimleri Dergisi* **2017**, *20*, 38-47; b) W. T. Gan, Y. Liu, L. K. Gao, X. X. Zhan, J. Li, *Ceram. Int.* **2015**, *41*, 14876-14885; c) N. Zhang, Y. Huang, M. Zong, X. Ding, S. P. Li, M. Y. Wang, *Ceram. Int.* **2016**, *42*, 18879-18886.
[11] a) O. Yalcin, H. Bayrakdar, S. Ozum, *J. Magn. Magn. Mater.* **2013**, *343*, 157–162; b) P. B. Liu, Y. Huang, X. Zhang, *Synth. Met.* **2015**, *201*, 76–81.
[12] a) A. A. Asgharinezhad, H. Ebrahimzadeh, *J. Chromatogr. A* **2015**, *1412*, 1–11; b) Y. Chen, Y. L. Wang, H. B. Zhang, X. F. Li, C. X. Gui, Z. Z. Yu, *Carbon* **2015**, *82*, 67–76.
[13] C. Y. Lee, H. G. Song, K. S. Jang, E. J. Oh, A. J. Epstein, J. Joo, *Synth. Met.* **1999**, *102*, 1346–1349.
[14] X. H. Ren, G. L. Xu, *J. Magn. Magn. Mater.* **2014**, *354*, 44–48.
[15] U. S. R. M. Cornell, *The iron oxides: Structure, properties, reactions, occurences and uses*, Weinheim: VCH Verlag, **1996**.
[16] a) N. Zhang, Y. Huang, M. Zong, X. Ding, S. P. Li, M. Y. Wang, *Chem. Eng. J.* **2017**, *308*, 214–221; b) L. A. Frolova, M. P. Derhachov, *Nanoscale Res. Lett.* **2017**, *12*, 1–9; c) Z. Liu, C. Wu, L. Niu, G. Yang, K. Wang, W. Pei, Q. Wang, *Nanoscale Res. Lett.* **2017**, *12*, 1–6.
[17] a) C. N. Chinnasamy, M. Senoue, B. Jeyadevan, O. Perales-Perez, K. Shinoda, K. Tohji, *J. Colloid Interface Sci.* **2003**, *263*, 80–83; b) G. Bisht, S. Rayamajhi, K. C. Biplab, S. N. Paudel, D. Karna, B. G. Shrestha, *Nanoscale Res. Lett.* **2016**, *11*, 1–11.
[18] X. D. Jin, Q. Q. Ni, Y. Q. Fu, L. Zhang, T. Natsuki, *Polym. Compos.* **2012**, *33*, 317–323.
[19] Y. Liu, D. Song, C. X. Wu, J. Leng, *Compos. B. Eng.* **2014**, *63*, 34–40.
[20] a) H. Mei, D. Y. Han, S. S. Xiao, T. M. Ji, J. Tang, L. F. Cheng, *Carbon* **2016**, *109*, 149–153; b) H. Mei, X. Zhao, J. C. Xia, F. Wei, D. Y. Han, S. S. Xiao, L. F. Cheng, *Mater. Des.* **2018**, *144*, 323–330; c) D. W. Lu, Z. C. Mo, B. H. Liang, L. L. Yang, Z. F. He, H. Zhu, Z. K. Tang, X. C. Gui, *Carbon* **2018**, *133*, 457–463; d) E. Z. Zhou, J. B. Xi, Y. Guo, Y. J. Liu, Z. Xu, L. Peng, W. W. Gao, J. Ying, Z. C. Chen, C. Gao, *Carbon* **2018**, *133*, 316–322.
[21] a) Y. Ahn, E. J. Choi, S. Kim, H. N. Ok, *Mater. Lett.* **2001**, *50*, 47–52; b) V. A. M. Brabers, *Phys. Status Solidi* **1969**, *33*, 563–572; c) A. Shokri, S. F. Shayesteh, K. Boustani, *Ceram. Int.* **2018**, *44*, 22092–22101.
[22] B. Smith, *Infrared Spectra Interpretation: A Systematic Approach*, CRC Press, New York, **1998**.
[23] R. Lamouri, M. Tadout, M. Hamedoun, A. Benyoussef, H. Ez-Zahraouy, M. Benaissa, O. Mounkachi, *J. Magn. Magn. Mater.* **2017**, *436*, 6–10.
[24] V. S. Kumbhar, A. D. Jagadale, N. M. Shinde, C. D. Lokhande, *Appl. Surf. Sci.* **2012**, *259*, 39–43.
[25] a) S. D. Topel, O. Topel, R. B. Bostancioglu, A. T. Koparal, *Colloids Surf. B* **2015**, *128*, 245–253; b) JCPDS, Joint Committee on Powder Diffraction Standards, Diffraction Data File No. 19-0629, Pennsylvania; c) Z. J. Zhang, X. Y. Chen, B. N. Wang, C. W. Shi, *J. Cryst. Growth* **2008**, *310*, 5453–5457; d) S. M. Taimoory, J. F. Trant, A. Rahdar, M. Aliahmad, F. Sadeghfar, M. Hashemzaei, *e-J. Surf. Sci. Nanotechnol.* **2017**, *15*, 31–39.
[26] a) K. Maaz, A. Mumtaz, S. K. Hasanain, A. Ceylan, *J. Magn. Magn. Mater.* **2007**, *308*, 289–295; b) Z. F. Zi, Y. P. Sun, X. B. Zhu, Z. R. Yang, J. M. Dai, W. H. Song, *J. Magn. Magn. Mater.* **2009**, *321*, 1251–1255; c) M. H. Habibi, H. J. Parhizkar, *Spectrochim. Acta Part A* **2014**, *127*, 102–106; d) S. Sagadevan, J. Podder, I. Das, *Springer Proc. Phys.* **2017**, *189*, 145–152.
[27] a) Y. Jia, D. H. Kim, T. Lee, S. Kang, B. W. Lee, S. J. Rhee, C. Liu, *RSC Adv.* **2016**, *6*, 76542–76550; b) H. Elmoussaoui, M. Hamedoun, O. Mounkachi,

A. Benyoussef, R. Masrour, E. K. Hlil, *J. Supercond. Novel Magn.* **2012**, *25*, 1995–2002.
[28] a) V. V. Mody, A. Singh, B. Wesley, *Eur. J. Nanomed.* **2013**, *5*, 11–21; b) A. H. Lu, E. L. Salabas, F. Schuth, *Angew. Chem. Int. Ed.* **2007**, *46*, 1222–1244.
[29] M. Houshiar, F. Zebhi, Z. J. Razi, A. Alidoust, Z. Askari, *J. Magn. Magn. Mater.* **2014**, *371*, 43–48.
[30] F. X. Liu, T. Z. Li, H. G. Zheng, *Phys. Lett. A* **2004**, *323*, 305–309.
[31] a) D. Carta, M. F. Casula, A. Falqui, D. Loche, G. Mountjoy, C. Sangregorio, A. Corrias, *J. Phys. Chem. C* **2009**, *113*, 8606–8615; b) N. Jahan, M. M. Uddin, M. N. I. Khan, F. U. Z. Chowdhury, M. R. Hasan, H. N. Das, M. M. Hossain, *J. Mater. Sci. Mater. Electron.* **2021**, *32*, 16528–16543.
[32] F. Mostaani, M. R. Moghbeli, H. Karimian, *J. Thermoplast. Compos. Mater.* **2018**, *31*, 1393–1415.
[33] R. Fallah, S. Hosseinabadi, G. Pourtaghi, *J. Environ. Health* **2022**, *20*, 113–122.
[34] N. Maruthi, M. Faisal, N. Raghavendra, B. P. Prasanna, S. R. Manohara, M. Revanasiddappa, *Synth. Met.* **2021**, *275*, 1–9.
[35] M. Jung, Y. S. Lee, S. G. Hong, J. Moon, *Cement. Concrete. Res.* **2020**, *131*, 1–15.
[36] J. Joseph, P. R. Munda, D. A. John, A. M. Sidpara, J. Paul, *Mater. Res. Express* **2019**, *6*, 085617.
[37] Y. Fan, L. Zhang, V. Volski, G. A. E. Vandenbosch, B. Blanpain, M. X. Guo, *Sci. Rep.* **2017**, *7*, 1–8.
[38] Y. Q. Tan, H. Luo, X. S. Zhou, S. M. Peng, H. B. Zhang, *Sci. Rep.* **2018**, *8*, 1–8.
[39] A. Ç A İ Kaya, *İleri Teknoloji Bilimleri Dergisi* **2016**, *2147*, 815–819.
[40] P. Saini, M. Arora, G. Gupta, B. K. Gupta, V. N. Singh, V. Choudhary, *Nanoscale* **2013**, *5*, 4330–4336.
[41] M. Chahar, S. Dabas, O. P. Thakur, *Ceram. Int.* **2022**, *48*, 5352–5360.

Manuscript received: October 12, 2023